Engineering Structures 178 (2019) 410–422

Contents lists available at ScienceDirect

Engineering Structures

journal homepage: www.elsevier.com/locate/engstruct

Experimental cyclic response of RC walls with setback discontinuities

Leonardo M. Massone[a,*], Sebastián Díaz[a], Ignacio Manríquez[a], Fabián Rojas[b], Ricardo Herrera[b]

[a] Department of Civil Engineering, University of Chile, Blanco Encalada 2002, Santiago, Chile
[b] Department of Civil Engineering, University of Chile, Santiago, Chile

ARTICLE INFO

Keywords:
Slender wall
Experiment
Flag walls
Cyclic loading
Discontinuities
Setback
Numerical model

ABSTRACT

After the 2010 Maule, Chile, earthquake (Mw 8.8), several reinforced concrete (RC) buildings presented damage in some walls (crushing of concrete, buckling and fracture of steel reinforcement). These buildings had been designed according to the up-to-date seismic standards in the country and were not expected to suffer damage as severe as what was observed. Common features of the damaged walls were: little or no confinement at the wall ends; relatively high axial load; narrow thicknesses (below 200 mm); and discontinuities in height. Slender RC walls are often used in Chile and commonly, due to architectural constraints, the length of the walls changes between floors designated for parking use and the upper floors, creating a setback in the lower levels. These types of walls are commonly called "flag walls". The problem of discontinuity has not been investigated experimentally and therefore it is necessary to observe its impact in RC walls. Four structural wall specimens were designed, one with no discontinuity and the other three with different sizes of the setback. They were tested under a nominal constant axial load of $0.1f'_cA_g$ and cyclic lateral loads increasing at specific drift levels. Conventional instrumentation and photogrammetry were used to monitor the tests. The experimental results show that the impact of the setback, for the sizes tested, is not significant for the strength but it is relevant for the strength degradation and deformation capacity. Strains in the extreme fibers, curvature and principal strains are studied using photogrammetry. It is found that the plastic hinge length increases with drift, but it remains constrained to the setback region. Another discontinuity is found around the reinforcement of the setback where large concentration of strains can cause premature failure of the wall.

1. Introduction

On February 27, 2010, an earthquake of magnitude 8.8 (Mw) hit Chile. While infrastructure largely performed well, several newer reinforced concrete buildings suffered damage in their reinforced concrete walls (concrete crushing, buckling and fracture of steel reinforcement). These buildings had been designed according to the up-to-date seismic standards in the country [1,2] and were not expected to suffer damage as severe as what was observed, particularly in cities some 400 km away from the main rupture zone. Common features of the damaged walls were: little or no confinement at the wall ends; relatively high axial load; narrow thickness (below 200 mm); and discontinuities in height. This last aspect has not been addressed by the modifications to the reinforced concrete Chilean code [2] issued after the earthquake [3]. In residential buildings, it is common due to architectural requirements that the length of walls is reduced at the lower floors destined for parking, causing a change in the extension of the wall between these and the upper floors and creating a setback at the edges of the building, commonly referred to as a "flag wall" configuration. Fig. 1 shows a schematic of this wall configuration and damage observed after the 2010 seismic event.

The effect of the degree of discontinuity at the base has not been studied experimentally and therefore is necessary to observe its impact on the structural performance of the wall. This paper presents the details and results of experiments on slender reinforced concrete walls with discontinuities of different sizes at the base. Photogrammetry equipment is used as part of the instrumentation to study the distribution of strain along the height of the building. The effect of the height and length of the discontinuity on the behavior of the plastic hinge formation and the distribution of curvature on its height is observed. Plastic hinge estimation is a key issue in current displacement-based design, which provides the detailing requirements in the wall boundary elements based on estimations of compressive strain demands.

* Corresponding author.
E-mail addresses: lmassone@ing.uchile.cl (L.M. Massone), frojas@ing.uchile.cl (F. Rojas), riherrer@ing.uchile.cl (R. Herrera).

https://doi.org/10.1016/j.engstruct.2018.10.054
Received 17 May 2017; Received in revised form 21 September 2018; Accepted 20 October 2018
Available online 25 October 2018

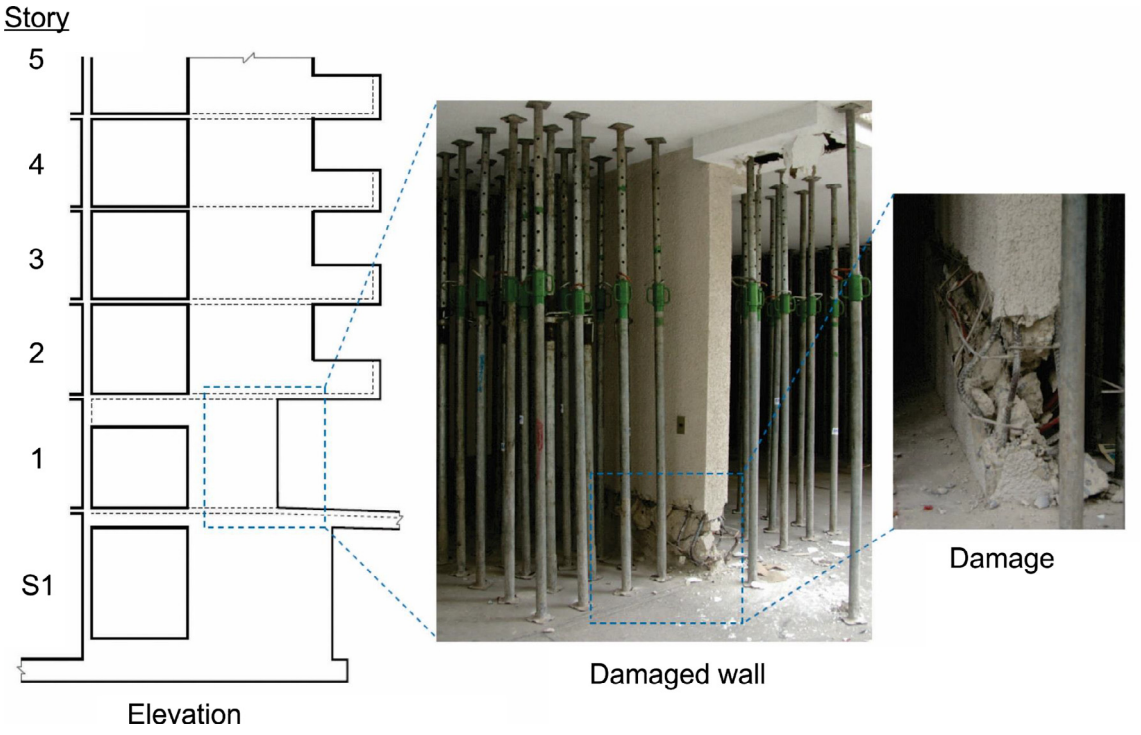

Fig. 1. Damage in walls with discontinuities in height after the 2010 earthquake.

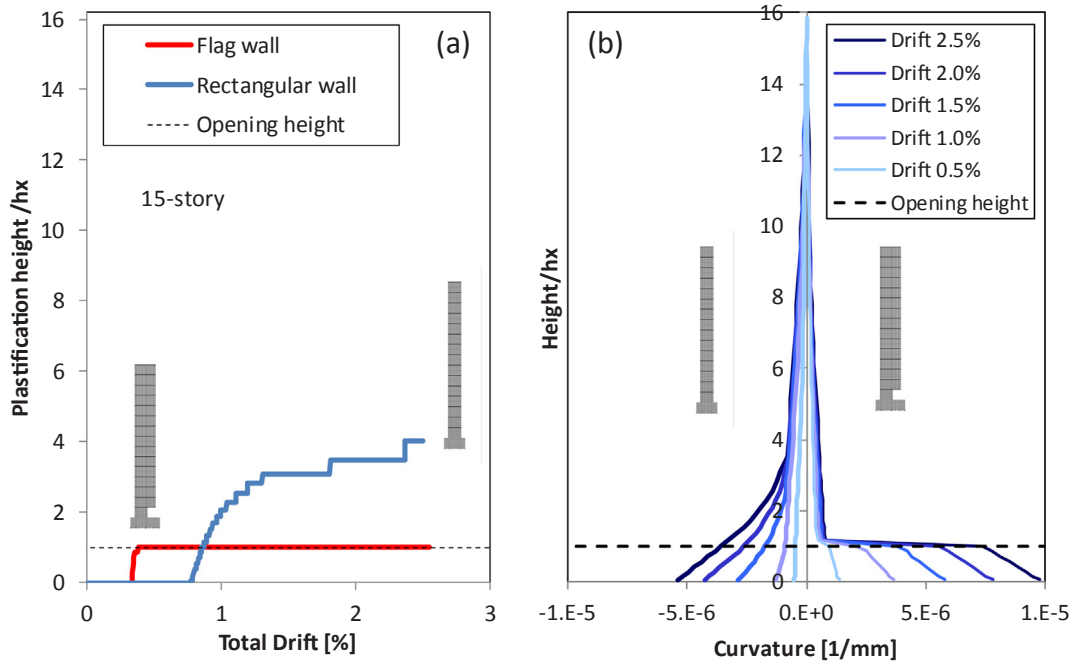

Fig. 2. Analytical results for a 15-story wall with discontinuity length of 20% (l_x/l_w = 0.2) [7] – (a) Plastification distribution versus drift, and (b) wall curvature distribution for rectangular and flag-wall.

2. Previous research

2.1. Walls with discontinuities

Previous research on the response of slender walls with discontinuities has focused in door or window openings [4,5], rather than in discontinuities due to setback. Taylor et al. [4] tested two scaled walls showing that slender walls with an opening at the base can have important ductility, as long as detailing is designed under a displacement-based approach. However, the presence of the discontinuity reduced the displacement capacity compared to the continuous wall. Ali and Wight [5] tested four scaled RC walls: three with staggered openings and one with no openings. The objective was to study the influence of the location of the openings. The staggered configuration was shown to be a better option than “in line” openings, similar to coupled walls, because less detailing near the openings was required. Results reveal that all specimens show stable behavior and large ductility, although with smaller ductility than the specimen without opening.

As an extension of the work by Massone and Alfaro [6], numerical

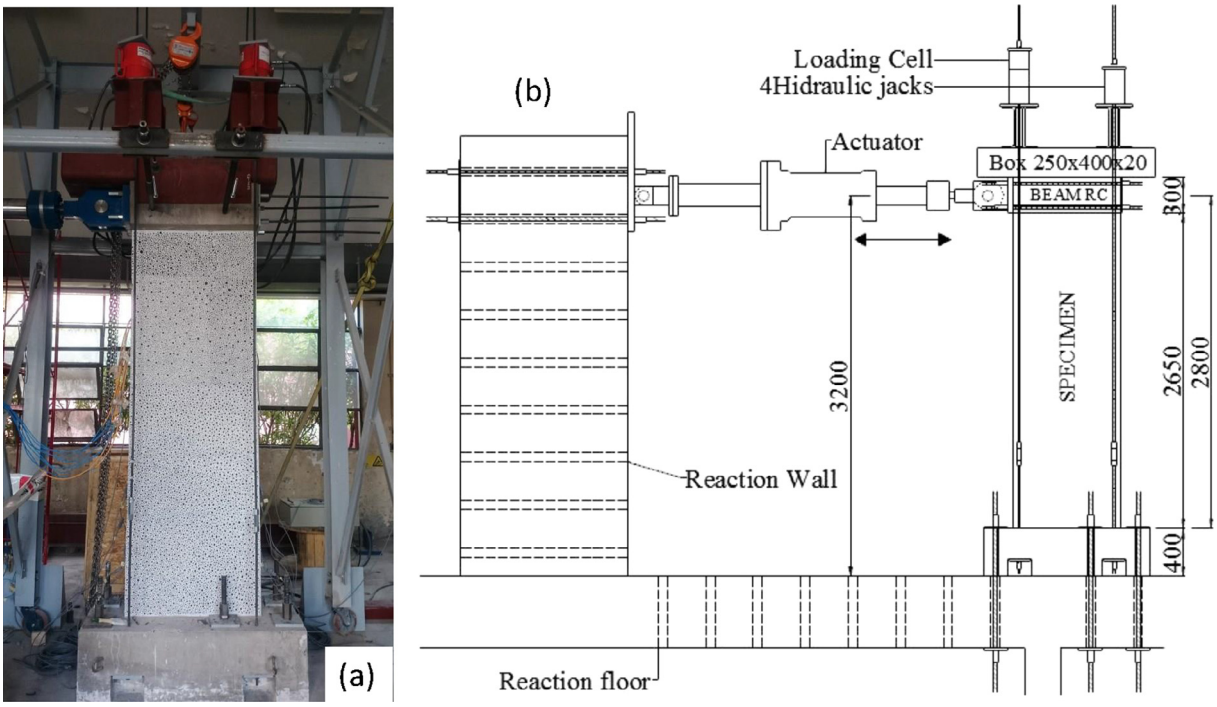

Fig. 3. Test assembly and scheme – (a) actual setup, and (b) global scheme.

analyses were conducted by Massone et al. [7] to study the impact on performance of the presence of a wall setback. The results focused on predictions of yield displacement, plastic hinge length, and base curvature. The study used fiber models of walls with a setback at the wall base (flag-wall). In the model, the wall cross-section was discretized identifying concrete and steel fibers (uniaxial constitutive material laws) and also the wall was discretized in elevation allowing 3 degrees of freedom per node (2D analysis) in order to capture the flexural and axial response. The setback was modeled as oversized cross-sections for different length and height for the discontinuity. A constant axial load was applied to the models, as well as, a lateral top load that was controlled with increasing lateral displacement (pushover analysis). The analytical results indicate that the length of the plastic hinge located at the base increases with the displacement at the top of the wall. In the case of rectangular walls [6], the curvature gradually increases along the height, whereas in walls with the presence of a setback discontinuity at the base the plastic hinge tends to concentrate within the discontinuity at the base [7]. In cases where the height of the discontinuity is larger (taller), behavior is similar to the case of a rectangular wall. In Fig. 2a the first yield point (point along the height at which the wall most tensioned steel reinforcement fiber yields) develops at a lower drift level for flag walls than for rectangular walls. Moreover, the plastification tends to concentrate within the height of the base discontinuity, while the entire upper section of the wall tends to behave as a rigid body. In this case, the plastification height is defined as the height through which the longitudinal reinforcement has reached yielding. Fig. 2b shows the curvature values calculated in each layer of elements constituting the flexural model for walls with and without discontinuity. The negative direction shows the results for the rectangular wall and the positive direction for the wall with a discontinuity. The results evidence the concentration of curvature for the latter.

2.2. Photogrammetry

Photogrammetry allows tracking the position of an object through a sequence of images. Using the images, the displacement of regions of the objects in two orthogonal axes perpendicular to the normal to the image can also be calculated. The basic unit of a digital image is the pixel and it defines the resolution of the displacement that can be measured using that image. Each pixel is described by a color, either in RGB format for color pictures or in grayscale. The movement of this color from pixel to pixel can then be tracked through a series of images taken sequentially and transformed into a displacement knowing the size of the surface area that a pixel covers.

One of the algorithms used to measure displacements from digital images is the *Digital Image Correlation* (DIC). In this algorithm, tracking of the position and deformation is done through correlation coefficients. Currently, there are software developed using this algorithm which can adequately describe the response of an element [8]. The software in this study is Ncorr [9], an open source 2D digital image correlation program developed to detect displacements and strains in structural mechanics and geotechnical problems [10]. The element to be monitored must be painted with a random pattern of different size dots to generate a texture. The program divides the image using a user-defined grid that repeats on all subsequent images. Once the image is divided, a neighborhood of dots must be defined in the reference image that will be tracked in the other images. The solution to the problem is found using two correlation factors: Cross Correlation factor (Ccc) and Least Square factor (Cls). Both factors follow the Inverse Compositional Gauss-Newton (IC-NR) algorithm to find a correlation of the neighborhood previously defined through a least squares fit. The Ccc factor finds a first location of the neighborhood in the images and the Cls factor optimizes a vector that includes displacements and strains until a defined tolerance is reached. When the neighborhood is optimum, the rest of the elements of the grid is completed. The strain is then obtained with the gradients of displacement. More details can be found in [11]. This tool has been used in elements under uniaxial loading [12], but it has not been tested in two-dimensional elements, such as reinforced concrete walls under cyclic loading, where cracks alternatively open and close.

3. Test program

3.1. Test setup

The test setup is similar to the one used by previous authors, such as Taylor et al. [4] and Ali and Wight [5]. The specimens were attached to a strong floor by post-tensioning bars placed at the wall foundation beam. A steel frame restrained out-of-plane movement of the wall through restrainers in contact with the loading beam. Fig. 3 presents an overall view and a schematic diagram of the test setup. All specimens were loaded with vertical and lateral loads. A nominal axial compression load equal to $0.1f'_cA_g$ ($0.081f'_cA_g$ for specimen W1, and $0.071f'_cA_g$ for specimens W2, W3 and W4, due to concrete strength variation) was applied through a system of four bars anchored to the foundation beam tensioned by four hydraulic jacks sitting atop a metallic beam placed on the loading beam to better distribute the load. This level of axial load is representative of the gravity load on walls in the first stories of reinforced concrete buildings between 15 and 20 stories high in Chile.

The lateral displacement was applied at a height of 2.8 m (measured from the base of the wall) by means of an actuator attached with posttensioning bars to the strong wall and to the loading beam on top of the wall. The actuator was pinned at both ends, had a capacity of 1000 kN, and a lateral displacement range of 50 cm. The specimens were subjected to the history of displacements shown in Fig. 4. This loading protocol was based on the recommendations of [13]. The displacements were applied quasi-statically until reaching severe damage.

3.2. Test specimens

Four reinforced concrete wall specimens (shown in Fig. 5), 2.65 m tall and 15 cm thick, were tested to verify the effect of the discontinuity over the performance of the walls. Specimen W1, the base case, was a 90 cm long rectangular wall, i.e. without discontinuity. Specimens W2, W3, and W4 kept the same base dimensions as W1, but had overhangs of different sizes at different wall heights (see Table 1). Specimen W2 had an opening of 250 mm in length and 300 mm in height. Specimen W3 had an opening with the same height, but doubled the length (500 mm). Specimen W4 had an opening of 250 mm in length and 600 mm in height to better distribute plasticity (according to previous analytical results [7], the higher the discontinuity, the closer the response is to a continuous wall, allowing tensile strains to distribute along the height of the wall boundary). All specimens had a 40x70 cm foundation beam to attach the specimen to the strong floor, a 30x40 cm loading beam on the top to apply the loads (vertical and lateral), and the same reinforcement configuration. Edge reinforcement was composed of 4-ϕ16 bars on both sides, with confinement provided by ϕ6 stirrups every 70 mm, over the bottom 1 m of the wall height. Similar reinforcement was provided on the hanging part of the wall for specimens W2, W3 and W4, composed of other 4-ϕ16 bars that act as continuation of boundary bars at the wall base on the discontinuous side.

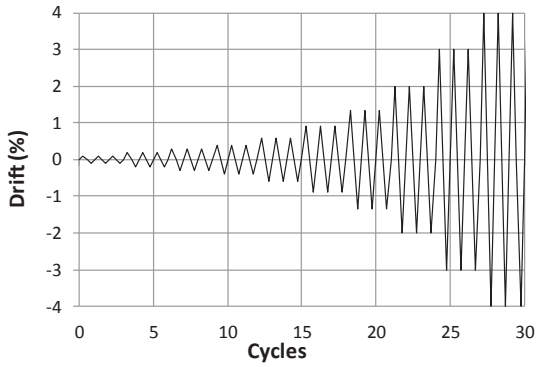

Fig. 4. Loading protocol.

The boundary bars on the discontinuous side are stop after a height of 1 m, resulting in extension of 0.7 m for specimens W2 and W3 within the upper part of the wall, which is sufficient anchorage for such reinforcement ($\sim 44d_b$, with d_b boundary bar diameter). In the case of specimen W4, the same height was maintained, resulting in an extension of only 0.4 m. The web of the walls was covered with ϕ8 bars every 200 mm, in both vertical and horizontal directions.

Four compartments were left on the underside of the foundation beam, to anchor the bars used to apply the vertical load, and 8 conduits spaced at 400 mm to leave space for the anchor rods to attach the beam to the strong floor. The loading beam had four conduits in the longitudinal direction to accommodate the bars that attached the beam to the actuator. The walls were cast off-site laying on the side of the discontinuity and were left to cure for at least 28 days. Formwork was removed after 7 days. The walls were then transported, in the same position that they were cast, to the Structural Testing Laboratory of the Department of Civil Engineering at the University of Chile to be tested. Once on site, they were unloaded and set in the vertical position in the final location for testing. All these operations were carried out with the walls lightly compressed by sling ropes to avoid unintended damage to the specimens. Limestone was placed underneath the foundation beam to provide a more uniform contact surface with the strong floor.

3.3. Material properties

Concrete and steel materials customary in Chile were used to fabricate the specimens. Concrete quality was H30 (f'_c = 25 MPa – nominal), reaching strengths of 33.0 MPa for W1 and a representative value of 38.3 MPa for W2, W3, and W4. A630-420H steel reinforcement bars were used, which are similar to grade 60 reinforcement (f_y = 420 MPa – nominal). The average measured yield stress for the ϕ8 bars was 493 MPa and for the ϕ16 bars was 496 MPa (see Table 2).

3.4. Instrumentation

Various instruments were used to measure load, strain, and displacements. Fourteen (14) strain gages were installed in the reinforcing bars, most of them at the base of the boundary longitudinal bars, and others placed on the horizontal reinforcement closest to the wall base, as shown in Fig. 6a. In addition, LVDTs were installed on the concrete wall surface both vertically and diagonally, in order to capture the flexural and shear components of deformation, as well as the top displacement and any pedestal movement (Fig. 6b). They varied between 25 and 32 sensors. Photogrammetry was used to monitor global and local (discontinuity region) displacements and strains of walls. The photogrammetry system used two cameras to capture images during the test at a constant frequency of 0.2 Hz of the entire wall and the bottom half of the wall to capture both the global response and local damage at the base. One face of the wall was whitewashed and then painted with a random pattern of varying size black dots (Fig. 6c). Further details regarding the installation and setup of the photogrammetry system and the image processing can be found in Manriquez [14].

4. Experimental response

All specimens were tested under the same axial load and lateral displacements, differing only by the size of the discontinuity at the base. Thus the capacity of all 4 specimens (W1, W2, W3, and W4) was similar, but they differed in the location and concentration of damage, which was noticeable at large drift levels (4%).

The initial behavior of all specimens was similar up to about 3% drift. The first distinguishable cracks appeared at the bottom of the wall during the third cycle at 0.3% drift in the negative direction (towards the reaction wall), and the number and width of cracks increased with the following cycles. Fig. 7 shows the lateral load versus lateral displacement response of the four specimens. The lateral displacement was

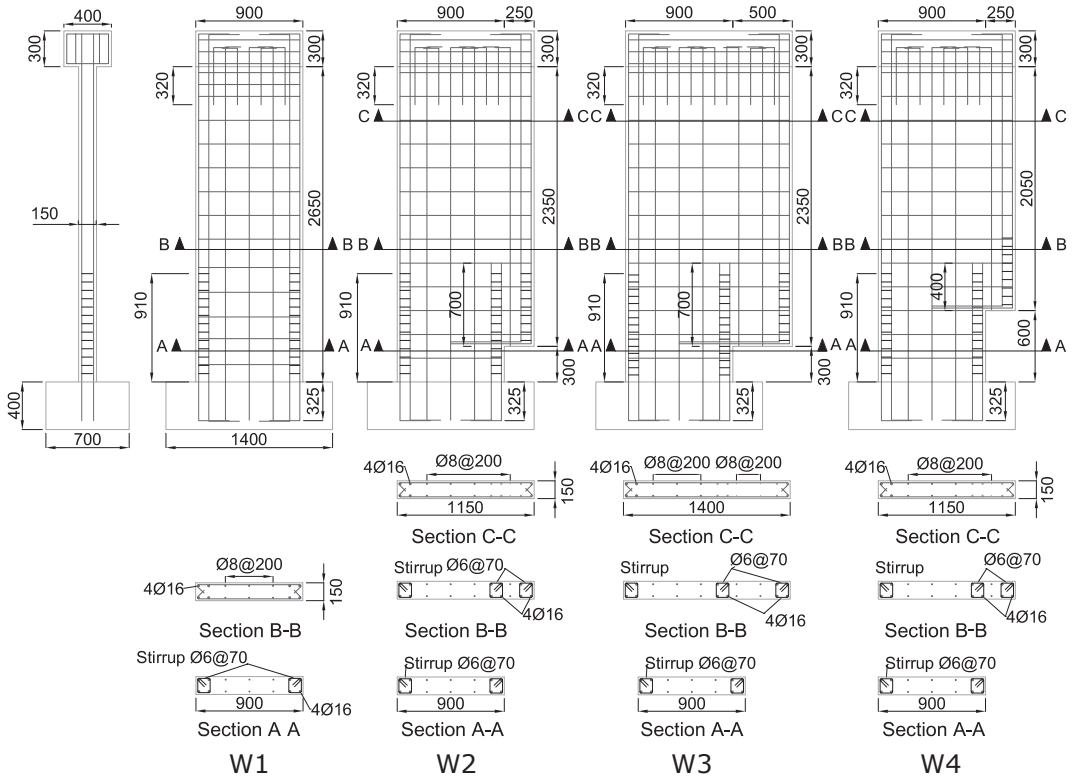

Fig. 5. Schematic of specimens (units in mm).

Table 1
Wall specimen characteristics.

Specimen	Height h_w [mm]	Total length l_w [mm]	Opening $h_x \times l_x$ [mm × mm]	Axial load P_o [kN]	Strength f'_c [MPa]	$P_o/A_g f'_c$ [%]
W1	2650	900	–	362	33	8.1
W2	2650	1150	300 × 250	365	38.3	7.1
W3	2650	1400	300 × 500	364	38.3	7.1
W4	2650	1150	600 × 250	367	38.3	7.1

Table 2
Reinforcing steel bars properties and distribution.

Reinforcing steel	Distribution	ρ** [%]	f_y [MPa]	f_u [MPa]
Boundary	4ϕ16	4.0	497	682
Distributed vertical	ϕ8@200 mm	0.32	494	631
Distributed horizontal	ϕ8@200 mm	0.34	494	631
Confinement	ϕ6@70 mm	0.54	280*	440*

ϕ: deformed bar diameter.
* Nominal properties.
** Considers actual tributary area.

determined at the location of the actuator, and corrected by the pedestal sliding and rotation. Load was applied first in the negative direction for all tests.

The presence of the discontinuity in the specimens W2 and W3 causes degradation in different drift cycles of 4%, before it happens with specimen W1 that does not have discontinuity. In the case of specimen W4 degradation is observed towards the end of the 3% drift cycle. More details of the response of each specimen are discussed next.

4.1. Specimen W1

The wall began to lose concrete cover at the wall boundaries during the first cycle at 3% drift in the negative direction, and diagonal cracks extended beyond half of the height of the wall. Strength degradation occurred in the third cycle at 4% drift in the positive direction, because of buckling of the boundary bars and crushing of concrete at the wall base on one of the edges. When going towards 6% drift level in the negative direction, the test was stopped at 4.5% drift because the specimen became unstable. The state of the wall at 2 and 3% drift and at the end of the test is shown in Fig. 8.

4.2. Specimen W2

The wall began to lose concrete cover during the first cycle of 3% drift in the negative direction (negative direction implies discontinuity zone in tension), which was noticeable on the side of the discontinuity. Diagonal cracks also extended over half the height of the wall, although concentrated at the bottom of the wall. Strength degradation occurred during the third cycle at 4% drift in the positive direction, at which point the bars were exposed and presented significant buckling, while concrete at the base of the wall on the edge was crushed. In addition, the boundary reinforcement on the compressed side fractured when changing direction. The state of the wall at 2 and 3% drift and at the end of the test is shown in Fig. 9.

4.3. Specimen W3

The wall began to lose concrete cover in the second cycle of 3% in the positive direction (positive direction implies discontinuity zone in compression), mostly at the wall boundary near the discontinuity region. Diagonal cracks were extended above half the wall height. Strength degradation occurred in the second cycle of 4% drift in the positive direction, presenting longitudinal bar buckling and concrete crushing at wall end. The second cycle at 4% was not completed because the bars fractured and strength degraded rapidly. The state of the wall at 3% drift and at the end of the test is shown in Fig. 10.

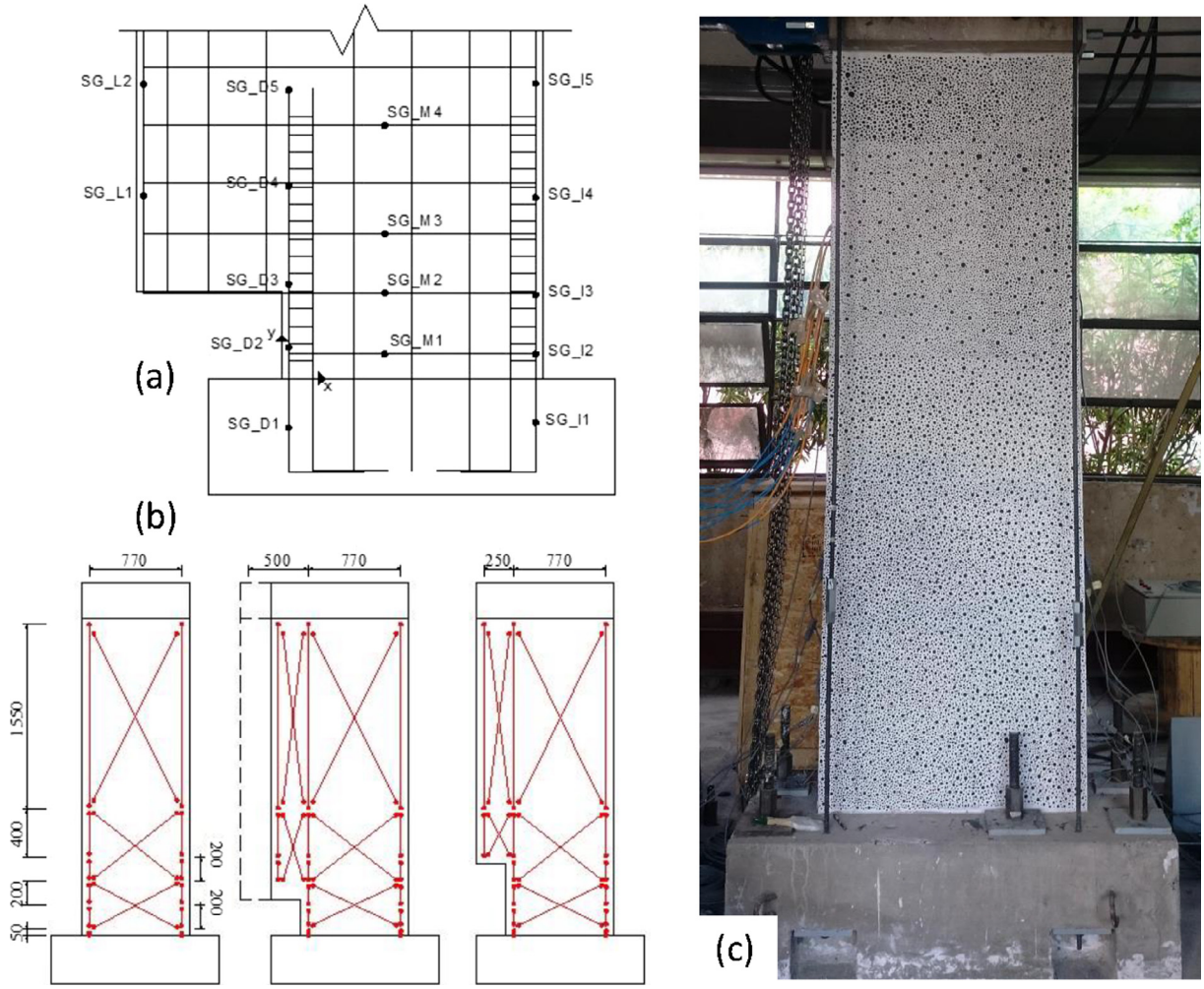

Fig. 6. Instrumentation scheme of wall specimens – (a) strain gages, (b) LVDTs, and (c) dot pattern for photogrammetry.

4.4. Specimen W4

At 2% drift, significant diagonal cracks appeared at a height of one meter, where the longitudinal boundary reinforcement was cut in the discontinuous side. Additionally, diagonal cracks could also be observed at the base level, although they were not as noticeable as the others. In the first cycle of 4% there was spalling of concrete where the boundary bar was discontinued. The damage present in this area was due to the insufficient anchoring of the boundary reinforcement, causing the reinforcement to slide and concentrate more deformation at this point, spalling the concrete more quickly and exposing both boundary, and vertical and horizontal web reinforcement. The test was stopped in the third cycle of the 4% drift in the negative direction (negative direction implies discontinuity zone in tension) since the capacity of the wall had been reduced remarkably. The cracks on the wall near the end of the boundary reinforcement at 3% drift and the state of the wall at the end of the test are shown in Fig. 11.

4.5. Measured wall strains

The data obtained by photogrammetry must be consistent with those recorded by the other sensors. There are studies that apply the DIC (Digital Image Correlation) algorithm to verify the associated error compared to strain gages and LVDTs (linear variable differential transducer). Within the studies, the consistency of the curvature in elements of reinforced concrete beams has been evaluated [15]. To verify the similarity of data between LVDTs and photogrammetry for the wall test program, a comparison of the data between both methods is carried out. At the general level, there is a LVDT located at 2.8 m height measured from the pedestal. As for photogrammetry, a sector (small) previously painted in the pedestal and the transfer beam are considered. Comparison of the top lateral displacement corrected by rigid body movement is performed up to the first cycle of 3% drift, which is shown in Fig. 12 for all four tests. In all specimens, high correlation of the data is observed, where a slope of the best fit (LVDT vs photogrammetry) presents a variation of less than 1% with respect to the perfect average estimation (45° diagonal), except for the case of specimen W4 that presents a difference of slope of 5%, due to the noise in the LVDT. Further efforts indicate that local strains can also be captured.

4.5.1. Maximum principal strains

The software used to measure displacements and strains with photogrammetry was Ncorr [9]. Figs. 13–16 present the principal strain values at 2% and 3% drift in both directions, using the same intensity scale. In all cases, the white sections represent either photo interference (anchor or post-tension bar) or wall discontinuity. Fig. 13 presents the strains measured for specimen W1. At 2% drift (Fig. 13a and b), the strains show symmetric distribution in height, with the largest strains occurring at the bottom of the wall. At 3% drift (Fig. 13c and d), the strains were distributed in a longer height than at 2% drift. In addition, the strains were significantly reduced above a height equivalent to the wall length (l_w).

Specimens W2 and W3 (Figs. 14 and 15, respectively) have a

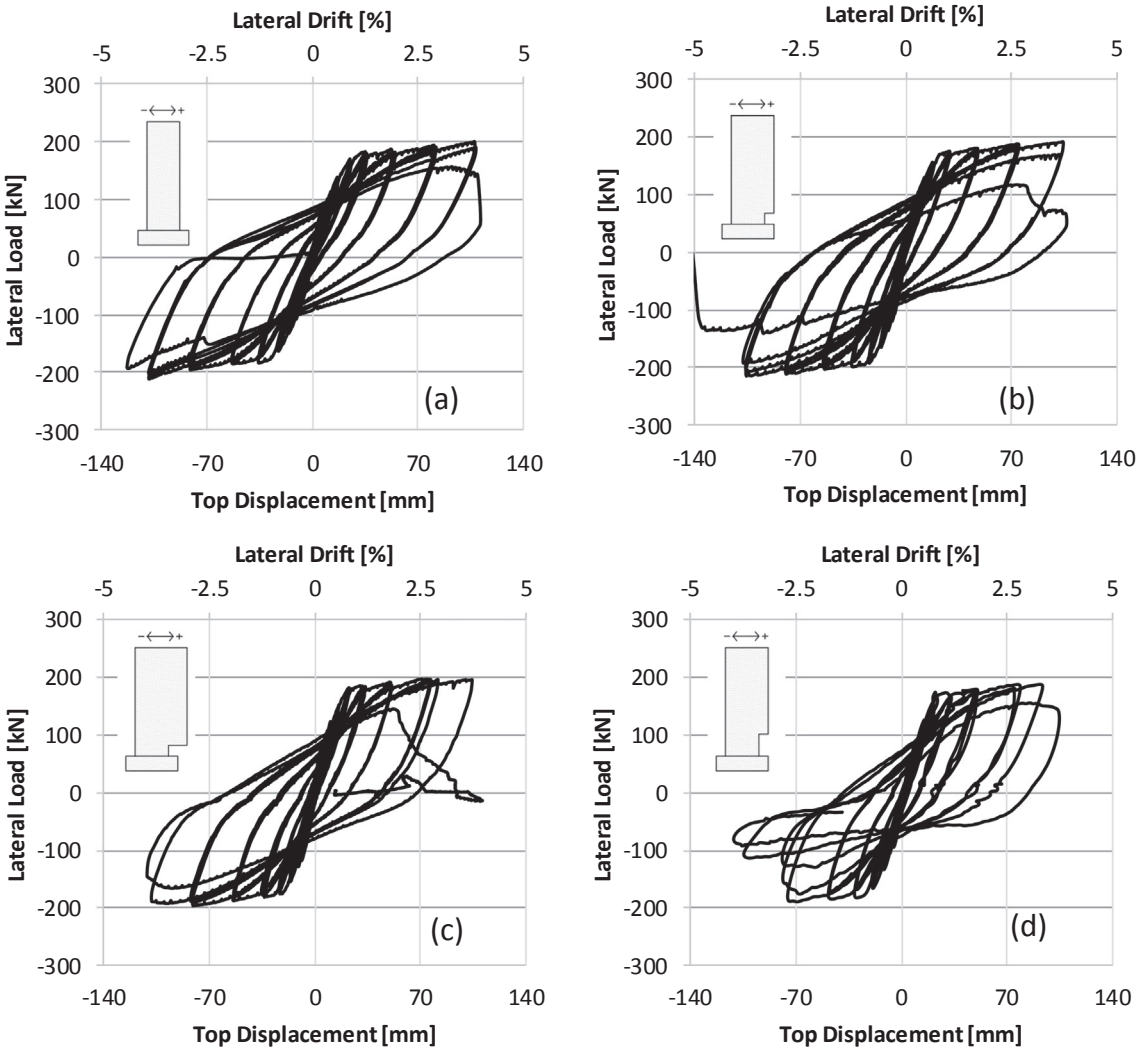

Fig. 7. Load displacement response of test specimens – (a) W1, (b) W2, (c) W3, and (d) W4.

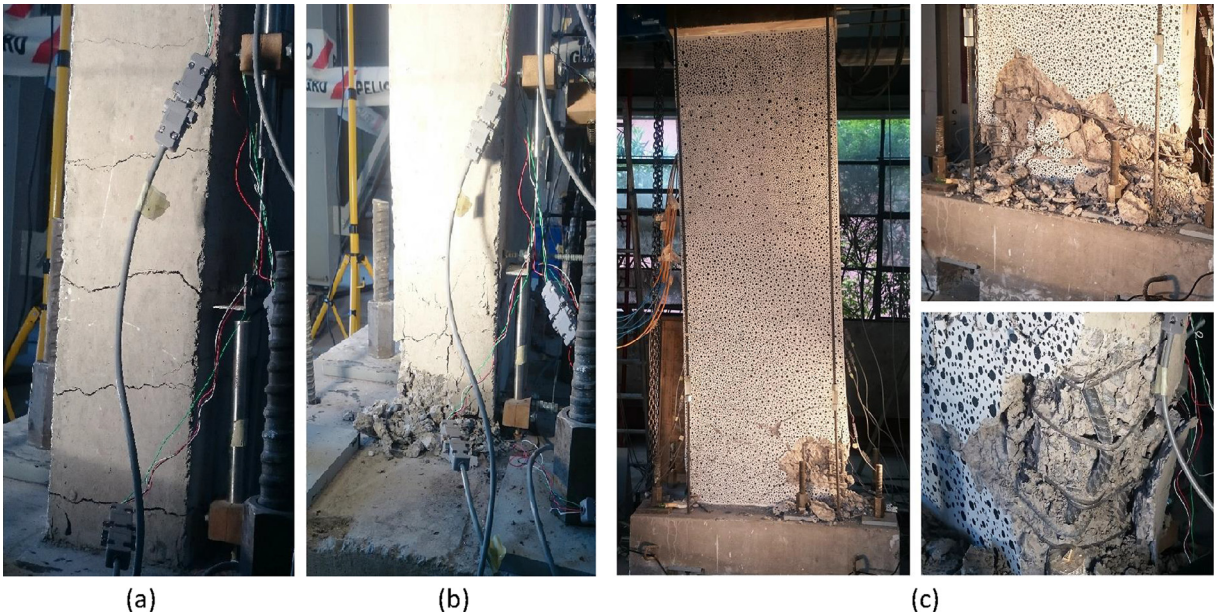

Fig. 8. Specimen W1 – (a) Cracking at 2% drift in the tension side for negative loading, (b) Spalling at 3% drift in the compression side for positive loading, and (c) final state.

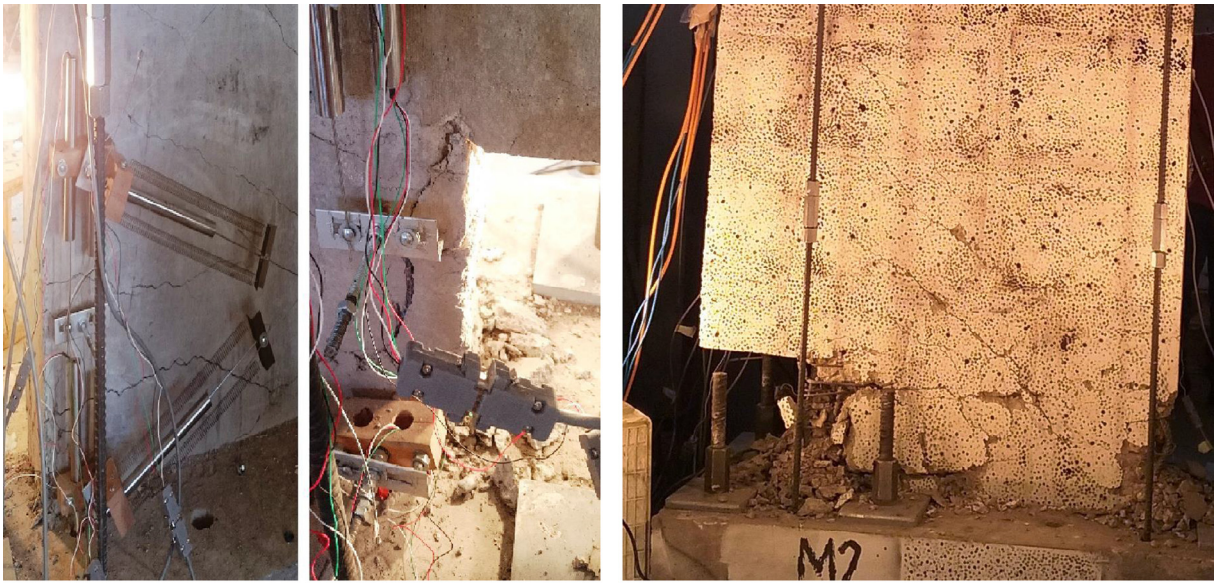

Fig. 9. Specimen W2 – (a) Cracking at 2% drift (continuous side), (b) damage at 3% drift (discontinuous side), and (c) final state.

slightly different behavior because larger strain values are observed within a height less than l_w, with significant strain concentration at a higher location that coincides with the end of the boundary reinforcement at the discontinuity region, when going in the negative direction (Figs. 14a, c and 15a, C). The strain field is distorted at such location. In the case of specimen W4 (Fig. 16a and c) this location is where strains are more concentrated and cracks are bigger than for the other specimens. Despite that, the cracks are concentrated on the base of the wall, near the discontinuity region. The distribution of cracks (indicated by light blue regions) is different for the positive and negative directions of loading. Positive directions always show better distribution of cracks in the wall. At 2% and 3% drift, strains show similar behavior for all specimens, without distinction between walls with or without discontinuity. (Figs. 13b, d; 14b, d; 15b, d; and 16b, d). Negative direction always show less cracks in the upper section of the wall (other than what is observed at the location of the discontinuous boundary bar). In general, at 2% and 3% drift, tensile strains show the biggest concentration in the discontinuous side (Figs. 14a, c; 15a, c; and 16a, c).

As was previously mentioned, degradation is observed in a previous cycle in specimens W2 and W3 compared with W1. The beginning of the degradation is due to the higher concentration of strains at the base according to the strain field within the discontinuity area. This can be observed at 3% drift in Figs. 14c, d and 15c, d (W2 and W3), that show larger concentration of warm colors (red – larger tensile strain values) at the discontinuity zone compared to the same location in Fig. 13c and d (W1).

4.5.2. *Distribution of vertical strains along the height*

The results from photogrammetry are also used to estimate the distribution of vertical strains. Fig. 17 shows vertical strains on the edge of specimens W1, W2, W3 and W4. Strains in the left side (negative) correspond to the tensile strains on discontinuous side when the wall is

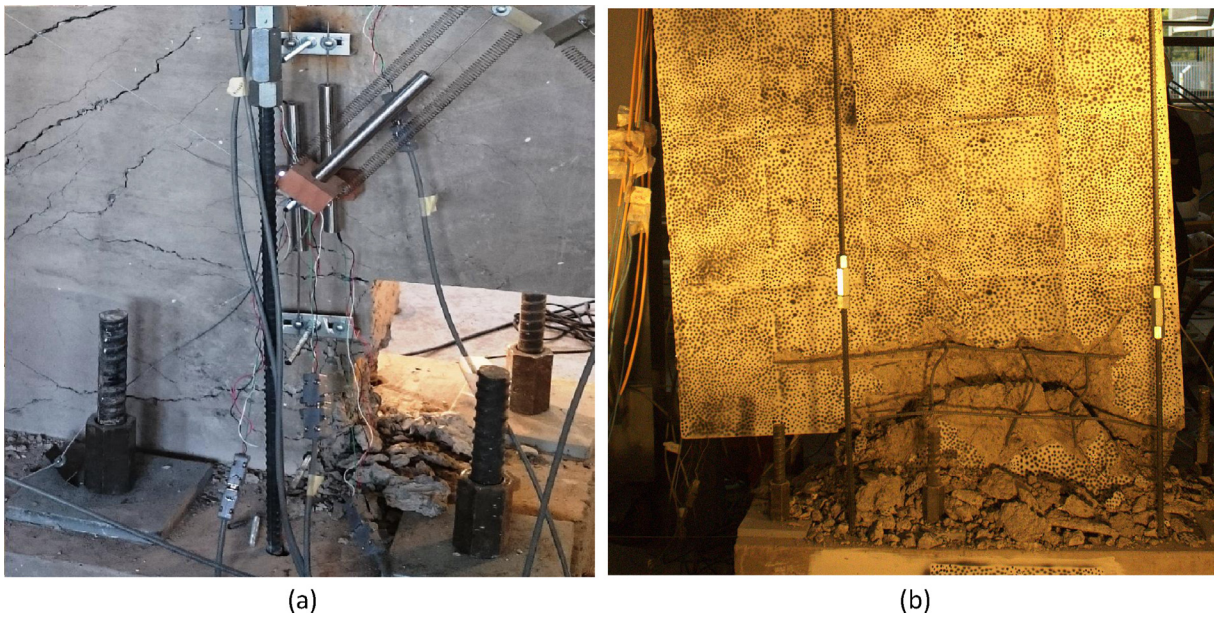

Fig. 10. Specimen W3 – (a) damage at 3% drift (discontinuous side), and (b) final state.

Fig. 11. Specimen W4 – (a) Cracks near the end of the boundary reinforcement at 3% drift (discontinuous side), and (b) final state.

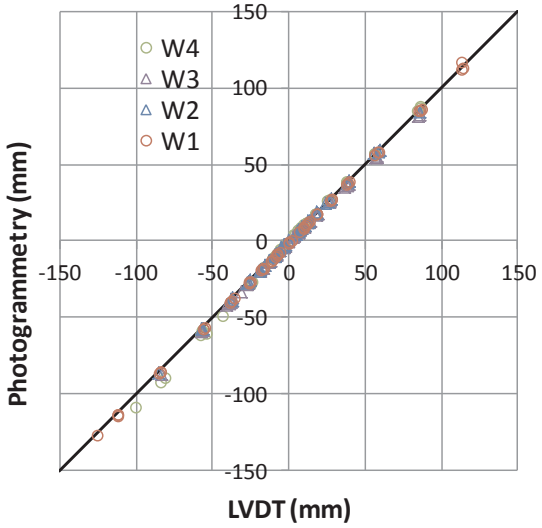

Fig. 12. Top lateral displacement comparison between LVDT and photogrammetry.

pushed in the negative direction. Positive strains correspond to the tensile strains on the continuous edge when the wall is pushed to the positive direction (for W1, due to the symmetry, the definition is not relevant). In the case of specimens W2, W3, and W4, the strains in the discontinuous side (negative loading) are measured at the same location along the height as for specimen W1. Fig. 17a shows a symmetric behavior with a strain concentration at the base for W1. The use of tensile strain (at boundary) was selected as a measure for the plastic hinge, since most nonlinearity comes from reinforcement yielding in tension and curvature estimation would require several calculations (neutral axis depth and equivalent curvature across the section due to deviation from Bernoulli hypothesis). For a constant neutral axis depth along the height of the wall, the use of tensile strain is a good estimate for plasticity distribution. The plastic hinge height is defined as the height at which the steel is above the measurement error (~0.004), which was selected as twice the yield strain (indicated by the vertical dashed lines in Fig. 17) as a close value. This was chosen since it was beyond yielding, and also, since for large drift values, below the point for this strain level, the curvature (tensile strain) grows to large values, which are only reduced at locations without cracks. Other similar selections of strain limit level would result in similar plastic hinge length.

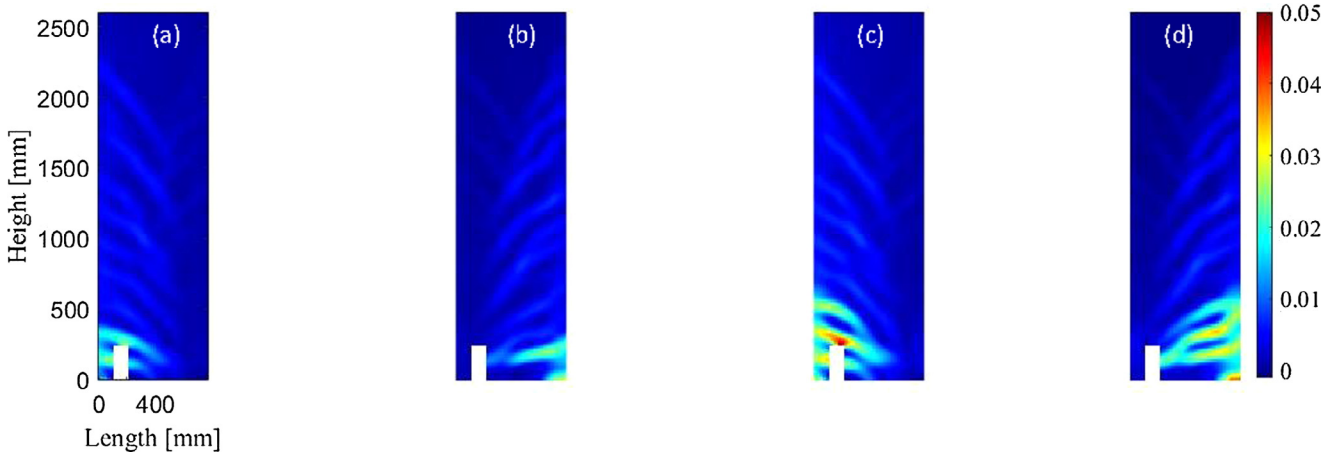

Fig. 13. Principal strain for specimen W1 by photogrammetry – (a and b) 2% drift; (c and d) 3% drift.

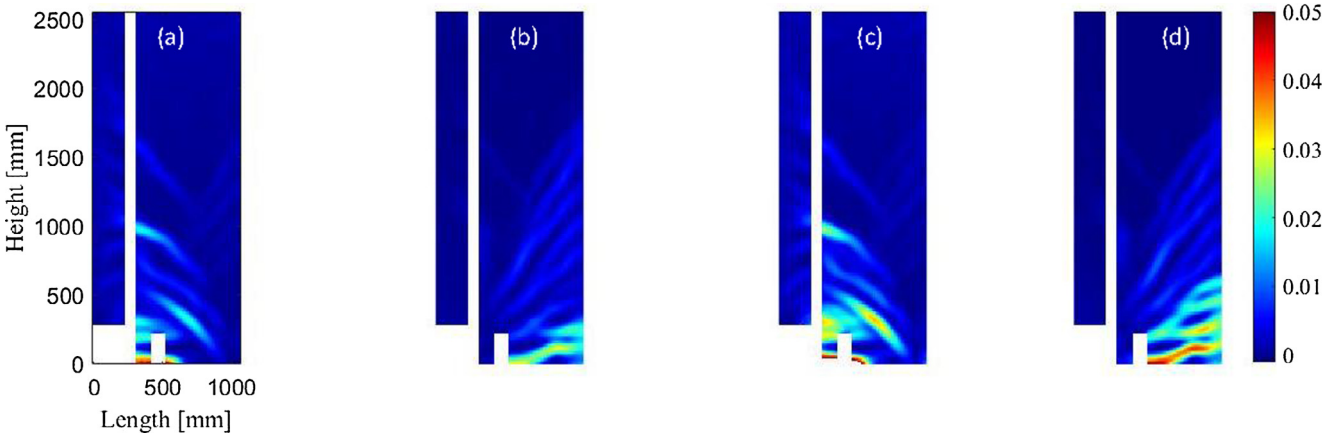

Fig. 14. Principal strain for specimen W2 by photogrammetry – (a and b) 2% drift; (c and d) 3% drift.

For example, if a value of $5\varepsilon_y$ is selected for the location of the plastic hinge, the length would be reduced by about 5% to 10%. Thus, the strain selection makes it a reasonable estimate for an equivalent plastic hinge length. Starting at 1.35% drift, an abrupt increase of strain is detected, attributed to the lengthening of the plastic hinge. At larger levels of drift, the plastic hinge reaches a higher height. The plastic hinge length reaches approximated values of 200 mm, 450 mm, and 700 mm at 1.35%, 2%, and 3% drift, respectively. This increment in plastic hinge length is consistent with Massone and Alfaro [6], where the plastic hinge length increases with the plastic drift level. Moreover, Fig. 17 also includes the location of the plastic hinge location (red dot) for 3% drift as well as the location of the discontinuity (h_x) as a dashed horizontal line. As it can be seen, above the location of the discontinuity the tensile strains tend to rapidly reduce (when the setback is under tension – negative side of the figure), close to the point of plastic hinge length definition. Other drift levels present smaller plasticity distribution, below h_x and similar to W1, indicating that they are not suitable to check the limitation of Eq. (1). Specimens W2, W3, and W4 (Fig. 17b–d) show similar strain magnitude, distribution and plastic hinge length to specimen W1 in the positive side of the plot. In all cases with setback (W2-4), the plastic hinge length in the positive direction is larger than in the negative direction, where for specimen W4 the differences are smaller given the larger height of the discontinuity (h_x) that almost does not affect the response. In the other hand, the negative direction shows a different behavior, with a more pronounced concentration of strains at the wall base and a peak strain value occurring at the beginning of the discontinuity (300 mm) for walls W2 and W3 (in W4 is less pronounced since the height of the discontinuity is 600 mm). A large strain value is also observed at the location of the end of the discontinuous longitudinal reinforcement (1000 mm). In general, the strain concentration at 1 m does not reveal an impact in the deformation or top lateral displacement contribution (except for W4), since the magnitude values are smaller than at wall base and covered a limited area (small rotation) and with a location that reduces the contribution to top displacement (rotation arm). In comparison with strains at the wall base, specimen W4 presents almost identical values at the base of the wall and at 1 m for large drift levels. Further concentration of tensile strain at the location of the discontinuous longitudinal reinforcement resulted in earlier strength degradation for specimen W4, but after reaching reinforcement yielding.

4.5.3. Plastic hinge length

Based on the work by Massone and Alfaro [6], Massone et al. [7] proposed that the plastic hinge length (l_p) increases with the plastic drift, but it remains constrained to the height of the discontinuity, h_x (Eq. (1)). This limitation is the only modification introduced for flag-walls.

$$l_p = (0.2l_w + 0.05z)\left(1 - \frac{1.5P}{f'_c A_g}\right)(6.7\Delta_p^{0.3}) \leq h_x \quad (1)$$

where the variable $z = M/V$ is the moment arm of the resultant lateral force, calculated as the moment-shear ratio at the plastic hinge location (assumed at the wall base), P is the applied axial force, f'_c is the compressive strength of concrete, A_g is the gross area of the wall, and Δ_p is the level of plastic drift, calculated as $\Delta_p = \frac{(\delta_u - \delta_y)}{h_w}$, where δ_y and δ_u are the yield and ultimate lateral displacements, respectively, and h_w is the wall height. The yield displacement was estimated as $\delta_y = 0.22\varnothing_y h_w^2$, whereas the yield curvature ($\varnothing_y$), which depends mainly on the yield strain (ε_y) and wall length (l_w), was determined as $\varnothing_y = 1.4\varepsilon_y/l_w$, as

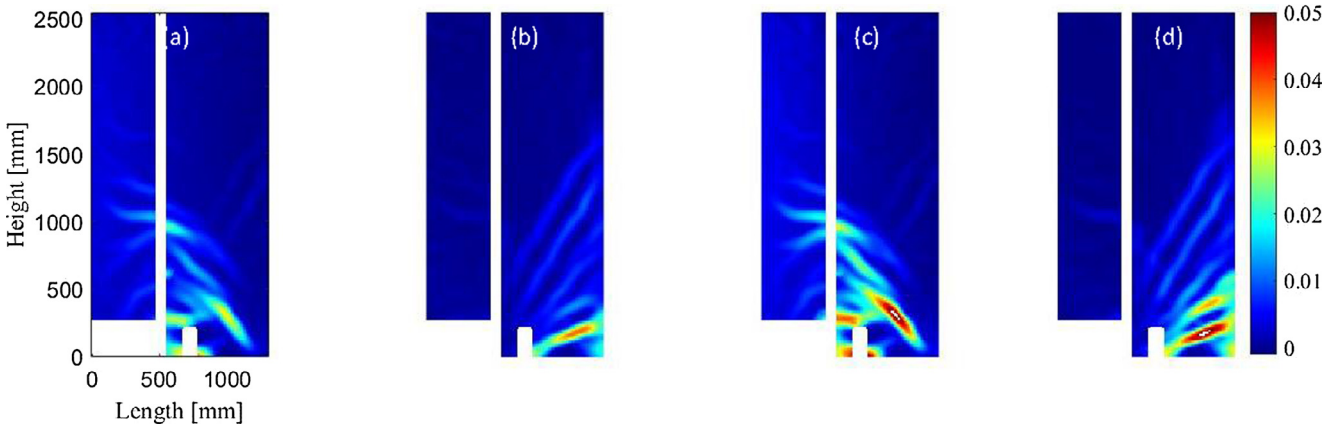

Fig. 15. Principal strain for specimen W3 by photogrammetry – (a and b) 2% drift; (c and d) 3% drift.

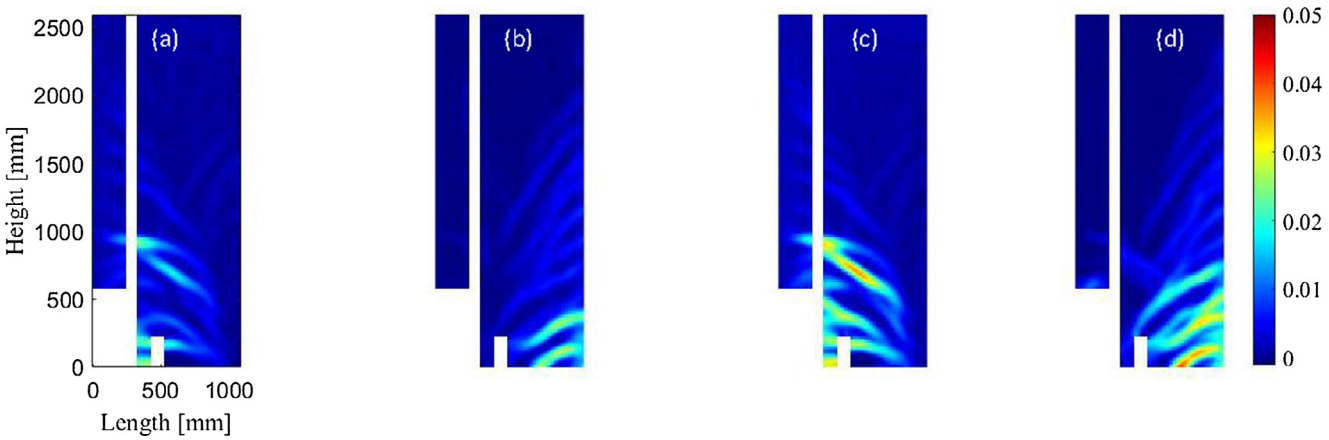

Fig. 16. Principal strain for specimen W4 by photogrammetry – (a and b) 2% drift; (c and d) 3% drift.

recommended by [6]. For all 4 specimens, only in specimen W1, the limit defined in Eq. (1) does not apply. In that case, the plastic hinge length is determined as 634 mm for a 3% lateral drift. For all other specimens (flag wall type) the limit (h_x, height of the discontinuity) controls, that is, 300 mm (W2 and W3) or 600 mm (W4) when the setback is under tension (negative side in Fig. 17). When the setback is under compression, similar values to W1 are obtained (~635 mm), which differ only due to differences in the real attained drift. The original expression for plastic hinge estimation [6] was determined for an equivalent rectangular (constant plastic curvature) curvature distribution and do not represent the point of initiation of yielding of longitudinal reinforcement. Most models for equivalent plastic hinge assume a constant curvature distribution, which for actual linear distribution of curvature below the yield point, results in a plastic hinge (or equivalent plastic hinge) of half the height to the point of yielding.

The plastic hinge length was determined from the photogrammetry data, using the same procedure as before, at 3% drift and the results were compared with the prediction from Massone et al. [7] (Fig. 18) for

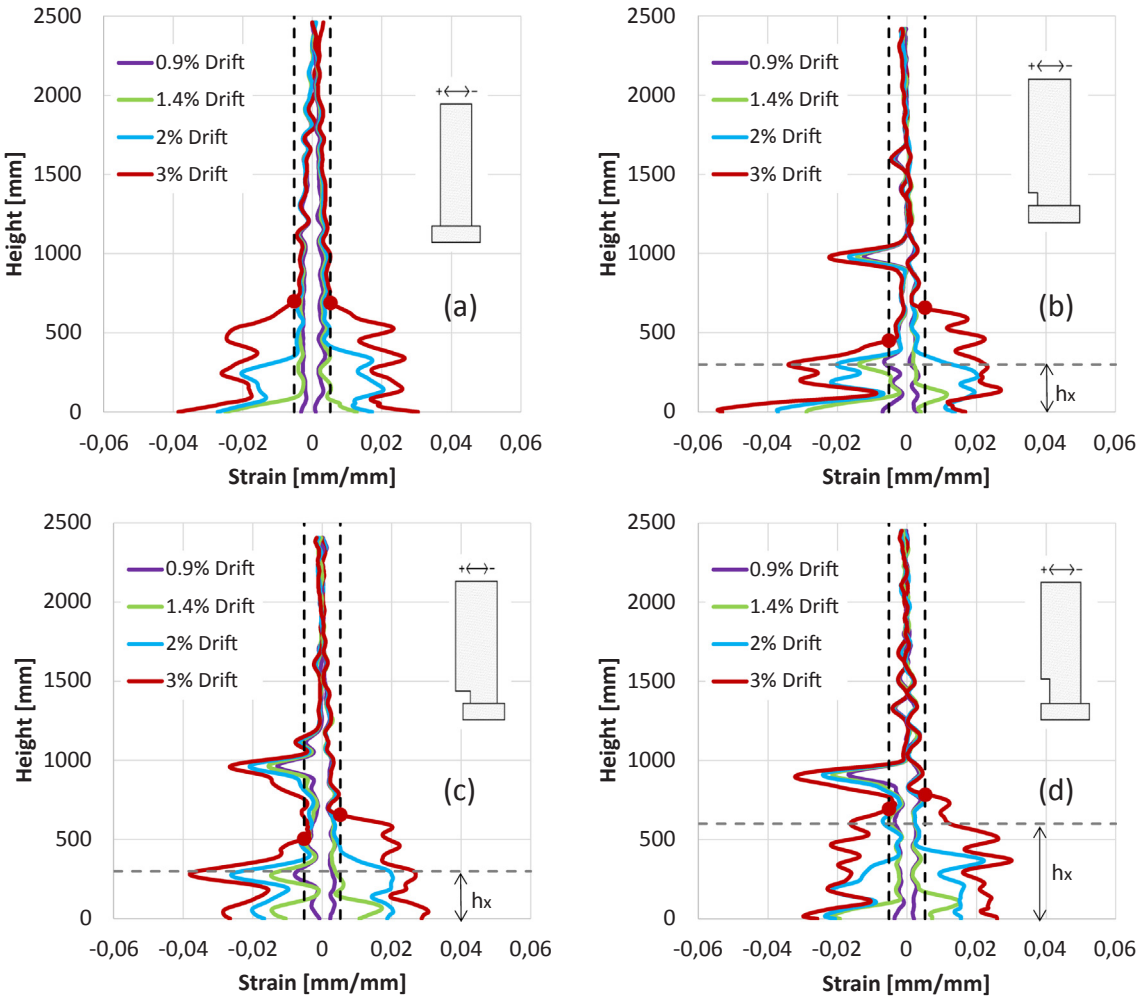

Fig. 17. Tensile vertical strain on extreme end at different drift levels for specimens – (a) W1, (b) W2, (c) W3, and (d) W4.

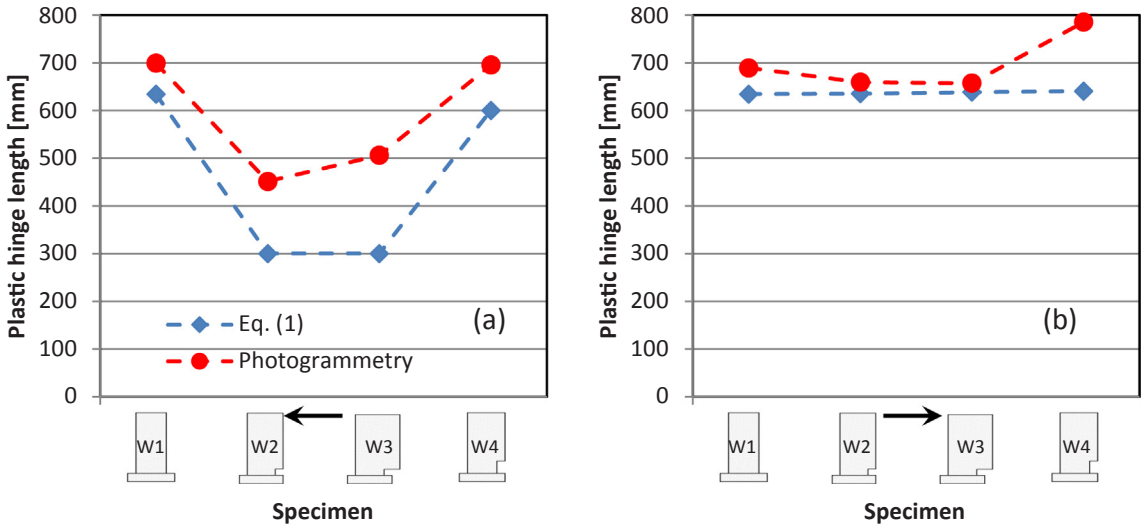

Fig. 18. Plastic hinge length at 3% drift, experiments vs. prediction for – (a) setback in tension and (b) setback in compression.

both loading directions. In the case of photogrammetry, the plastic hinge length was estimated from the strain distribution in the discontinuous side when it was in tension (for flag-wall cases), which is depicted in Fig. 18a. This indicates that there could be different plastic hinge lengths for flag walls depending on the loading direction, which in turns explains why there is a preferred direction for damage formation. Similar results are shown for the discontinuos side under compression in Fig. 18b. In the case of W1, results are almost identical due to its symmetry. Considering that the measurement error is about 0.004, initiation of the plastic hinge was determined once twice the yield strain was achieved (at the discontinuous boundary for specimens W2, W3 and W4), and the plastic hinge length as the length below this point. At large drift levels, it is clear that the plastic hinge has formed, and strains (and therefore curvature) tend to be relatively large with strain reduction at locations without cracks, which makes the length definition an ideal candidate for the equivalent plastic hinge length. As it can be seen in Fig. 18a, there is consistent correlation of the plastic hinge estimation and the measurement with photogrammetry when the setback is under tension (negative side in Fig. 17), reducing the plastic hinge length in cases where a small discontinuity is present (W2 and W3), which in turns implies larger curvature values at wall base. In this two cases, the model anticipates a plastic hinge length of 300 mm (height of the discontinuity), whereas the photogrammetry provides values of 451 mm and 506 mm, respectively. These values, although larger than the discontinuity height are similar between them and much smaller than what is estimated (634 mm) and measured (694 mm) for specimen W1. In the case of the taller discontinuity (W4) the measured plastic hinge length (695 mm) was similar to the rectangular wall (W1), and larger than for specimens W2 and W3, since damage was almost not affected or bounded by the discontinuity. Similar to specimens W2 and W3, the measured plastic hinge length for W4 (695 mm) resulted in a larger length (slightly in this case) than the discontinuity length (600 mm), supporting the idea that the discontinuity changes the distribution of curvature, but for large discontinuity length, the behavior of continuous wall (W1) is almost recovered. For the cases when the setback is under compression (Fig. 18b), specimens W2, W3 and W4 present a plastic hinge length of about 700 mm, similar to W1, supporting the idea that in such direction the response of those wall is similar to a continuous wall. According to the previous results, setting the plastic hinge length no larger than the discontinuity height when the setback is under tension would be conservative in displacement-based design providing larger curvature estimates, and a better approach than not taking into consideration the discontinuity.

5. Conclusions

Walls with discontinuities as setback (flag-wall) are common in Chile (due to architectural requirements, such as parking space at first stories or basement with fixed wall length) and other places, but little information on their behavior is available. Based on the results of previous analytical research, the length of the plastic hinge located at the base increases with the wall top displacement. In the case of rectangular walls, the curvature gradually increases in height, whereas in walls with the presence of discontinuity (setback) at the base, the plastic hinge tends to concentrate at the base.

In order to understand the behavior of walls with setback discontinuities and validate previous numerical simulations, four specimens with different discontinuities were constructed and tested under cyclic loads and a constant nominal axial force of $0.1f'_cA_g$. All specimens showed a similar load versus top displacement response, presenting strength degradation after reaching the first cycle of 4% drift. In the rectangular specimen (W1), strength degradation started at 4% drift, but in later cycles than the walls with discontinuities (W2, W3, and W4).

Analysis of strains in walls was performed using photogrammetry. In specimen W1, the largest strains were observed at wall base, but significant strains were also observed over almost the entire wall height. For walls with an opening (W2, W3, and W4) when loaded in the positive direction, the significant strains were also located at the bottom of the wall, with a similar distribution as for specimen W1. In the negative direction, there were significant tensile strains at the wall base, but tended to be enclosed within the discontinuous zone. There was also a significant tensile strain at the end of the longitudinal reinforcement that was discontinuous above the opening. Initiation of strength degradation indicated that the discontinuity concentrated the damage closer to the base of the wall, forcing the degradation to occur at the same level of displacement, but at an earlier cycle. Inadequate anchorage of specimen W4 resulted in damage concentration at the bar discontinuity and degradation at an even earlier cycle.

Estimation of plastic hinge formation in walls indicated that discontinuities tend to concentrate tensile strains, resulting in smaller hinge length for specimens with smaller discontinuity height. When the continuous side of the wall was in tension, crack distribution was similar to the rectangular wall indicating that the damage behavior (and plastic hinge length) was similar.

Acknowledgements

This work was financially supported by FONDECYT [grant N°1130219]. The help with the specimens testing of Mr. Ernesto Inzunza, Mr. Victor González, and Mr. Pedro Soto are also thanked.

Appendix A. Supplementary material

Supplementary data to this article can be found online at https://doi.org/10.1016/j.engstruct.2018.10.054.

References

[1] INN. NCh 433Of.1996: earthquake resistant design of buildings. Santiago, Chile: Instituto Nacional de Normalización; 2009. [in Spanish].
[2] INN. NCh 430Of.2008: reinforced concrete – design and calculation requirements. Santiago, Chile: Instituto Nacional de Normalización; 2008. [in Spanish].
[3] MINVU. D.S. N°60: Design and calculations requirements for reinforced concrete. Santiago, Chile: Ministerio de Vivienda y Urbanismo; 2011. [in Spanish].
[4] Taylor C, Cote P, Wallace J. Design of slender reinforced concrete walls with openings. Technical paper title no. 95–S39. ACI Struct J 1998;95(4):420–33.
[5] Ali A, Wight J. Reinforced concrete structural walls with staggered opening configurations under reverse cyclic loading. Report No. UMCE 90-05, Department of Civil Engineering, University of Michigan, Ann Arbor, Michigan; 1990.
[6] Massone LM, Alfaro JI. Displacement and curvature estimation for the design of reinforced concrete slender walls. Struct Design Tall Spec Build 2016;25(16):823–41.
[7] Massone LM, Rojas FR, Ahumada MG. Analytical study of the response of reinforced concrete walls with discontinuities of flag-wall type. Struct Concr 2017;18:962–73.
[8] Citrón R, Saouma V. Strain measurements with the digital image correlation system Vic-2D. Center of Fast Hybrid Testing, Department of Civil Environmental and Architectural Engineering, University of Colorado; 2008. CU/NEES-08-06.
[9] Blaber J, Adair B, Antoniou A. Ncorr: open-source 2D digital image correlation matlab software. Exp Mech 2015;55(6):1105–22.
[10] Stanier SA, Blaber J, Take WA, White D. Improved image-based deformation measurement for geotechnical applications. Can Geotech J 2016;53(5):727–39.
[11] Pan B, Asundi A, Xie H, Gao J. Digital image correlation using iterative least squares and pointwise least squares for displacement field and strain field measurements. Opt Lasers Eng 2009;47(7–8):865–74.
[12] Harilal R, Ramji M. Adaptation of open source 2D DIC software ncorr for solid mechanics applications. Proceedings of the 9th International Symposium on Advanced Science and Technology in Experimental Mechanics, 1–6 November, New Delhi, India. 2014.
[13] ACI T1.1-01. Acceptance criteria for moment frames base on structural testing. Farmington Hills, MI, USA: American Concrete Institute; 2001.
[14] Manriquez I. Reinforced concrete flag-wall tests under cyclic lateral loading measured with photogrammetry and strut-and-tie comparison. Santiago, Chile: Master thesis in Earthquake Engineering, Universidad de Chile; 2016. [in Spanish].
[15] Dutton M, Take WA, Hoult NA. Curvature monitoring of beams using digital image correlation. J Bridge Eng 2014;19(3):1–13.